

https://dspace.org/

Coherent Seismic Anisotropy Pattern Across Southern Africa Revealed by Shear Wave Splitting Measurements

Elamahalala Andriampenomanana Ny Ony; Andrew Nyblade; Raymond Durrheim; M van der Meijde; H Paulssen ...

https://hdl.handle.net/10539/40980
WOS

Downloaded from a DSpace repository. https://dspace.org/

Check for updates

AGU ADVANCING EARTH AND SPACE SCIENCES

Earth and Space Science

RESEARCH ARTICLE
10.1029/2023EA003469

Coherent Seismic Anisotropy Pattern Across Southern Africa Revealed by Shear Wave Splitting Measurements

Fenitra Andriampenomanana[1], Andrew Nyblade[1,2], Raymond Durrheim[1], Mark van der Meijde[3], Hanneke Paulssen[4], Motsamai Kwadiba[5], Onkgopotse Ntibinyane[5], Nortin Titus[6], and Mako Sitali[6]

[1]School of Geosciences, University of Witwatersrand, Johannesburg, South Africa, [2]Department of Geosciences, Pennsylvania State University, University Park, PA, USA, [3]University of Twente, Enschede, The Netherlands, [4]Utrecht University, Utrecht, The Netherlands, [5]Botswana Geosciences Institute, Lobatse, Botswana, [6]Geological Survey of Namibia, Windhoek, Namibia

Abstract We report new PKS, SKS, and SKKS splitting measurements for 88 seismic stations in Namibia, Botswana, South Africa, and Mozambique. When combined with measurements from previous studies, the ensemble of measurements shows a fairly uniform NNE to NE (~41° on average) fast-polarization direction (ϕ) and delay time (δt) (~0.7 s on average) across the entire southern African subcontinent. It is difficult to attribute the NNE-NE ϕ direction to just one source of anisotropy either within the lithospheric or sublithospheric mantle. We instead propose the observed anisotropy pattern could result from a combination of several sources that together give rise to a pervasive NNE-NE ϕ direction; (a) fossil anisotropy in the lithospheric mantle resulting from the Neoproterozoic collision of the Congo and Kalahari cratons to form the Damara Belt, (b) movement of the African plate over the asthenosphere, and (c) flow in the upper mantle induced by the African Superplume. In addition, a contribution from anisotropy in the lowermost mantle in the vicinity of the African large low shear velocity province cannot be ruled out.

Plain Language Summary Seismic anisotropy, or the directional dependence in seismic wave speed, reveals the ancient to present orientation of deformation of Earth's interior. In this study, shear waves refracted through the outer core and recorded at 88 seismic stations located in Namibia, Botswana, South Africa, and Mozambique were measured to constrain the anisotropic structure of the upper mantle beneath southern Africa. Our results, combined with previous results, show a consistent NNE-NE fast polarization direction. This direction cannot be easily explained by a single source of anisotropy caused either by past collisions of different geological blocks in southern Africa or the present movement of the African plate. Instead, we propose the pattern may result from a combination of three sources, (a) ancient deformation preserved within the deep continental lithosphere developed when the Congo and Kalahari cratons collided, (b) movement of the African plate over the asthenosphere, and (c) the flow of upwelling rock in the mantle beneath Africa.

Key Points:

- Shear wave splitting measurement across southern Africa shows a fairly uniform NNE to NE fast-polarization direction (ϕ)
- The observed ϕ direction cannot be easily attributed to just one source of anisotropy within the lithospheric or sublithospheric mantle
- The ϕ pattern may reflect several geodynamic processes

Supporting Information:

Supporting Information may be found in the online version of this article.

Correspondence to:

F. Andriampenomanana,
nyonyfenitra@gmail.com

Citation:

Andriampenomanana, F., Nyblade, A., Durrheim, R., van der Meijde, M., Paulssen, H., Kwadiba, M., et al. (2024). Coherent seismic anisotropy pattern across southern Africa revealed by shear wave splitting measurements. *Earth and Space Science*, *11*, e2023EA003469. https://doi.org/10.1029/2023EA003469

Received 6 DEC 2023
Accepted 29 APR 2024

Author Contributions:

Conceptualization: Fenitra Andriampenomanana, Andrew Nyblade
Data curation: Mark van der Meijde, Hanneke Paulssen, Motsamai Kwadiba, Onkgopotse Ntibinyane, Nortin Titus, Mako Sitali
Formal analysis: Fenitra Andriampenomanana
Methodology: Fenitra Andriampenomanana
Supervision: Andrew Nyblade, Raymond Durrheim
Writing – original draft: Fenitra Andriampenomanana
Writing – review & editing: Andrew Nyblade, Raymond Durrheim, Mark van der Meijde, Hanneke Paulssen

© 2024. The Author(s).
This is an open access article under the terms of the Creative Commons Attribution License, which permits use, distribution and reproduction in any medium, provided the original work is properly cited.

1. Introduction

Studies of seismic anisotropy have been used effectively for several decades to investigate the history of mantle deformation globally. In the upper mantle, deformation from tectonic processes can reorient olivine crystals through dislocation creep, creating an anisotropic fabric resulting from the lattice-preferred orientation (LPO) of olivine (e.g., Nicolas & Christensen, 1987; Savage, 1999; Silver & Chan, 1991). Seismic anisotropy in the lithospheric mantle can also arise from the shape-preferred orientation (SPO) of aligned inclusions or pockets of melt, or from faults and shear zones (e.g., Kendall et al., 2006; Savage, 1999). Common measurements used to quantify the anisotropic fabric of the upper mantle are the fast polarization direction (ϕ), which is the polarization azimuth of the fast shear wave measured in degrees clockwise from north, and the delay time (δt) measured in seconds between faster and slower polarized shear waves traversing through an anisotropic upper mantle, which is related to the strength and depth extent of the anisotropic layer(s). The two parameters, ϕ and δt, are commonly measured on broadband seismic data using the Rotation-Correlation (RC) method (Bowman & Ando, 1987) and/or the Minimum Energy (ME) method (Silver & Chan, 1991).

Some of the earliest shear wave splitting studies in southern Africa used data from permanent seismic stations and reported a NE ϕ direction, which was attributed to an anisotropic fabric in the sublithospheric mantle induced by absolute plate motion (APM) (e.g., Barruol & Ben Ismail, 2001; Helffrich et al., 1994; Vinnik

23335084, 2024, 5, Downloaded from https://agupubs.onlinelibrary.wiley.com/doi/10.1029/2023EA003469 by South African Medical Research, Wiley Online Library on [16/05/2024]. See the Terms and Conditions (https://onlinelibrary.wiley.com/terms-and-conditions) on Wiley Online Library for rules of use; OA articles are governed by the applicable Creative Commons License

et al., 1992). Barruol and Ben Ismail (2001), in addition, noted the alignment of the NE ϕ direction with NE-trending hotspot tracks on the African plate, and suggested that present-day plate motion, which presently moves in a NE direction with a speed of about 2–3 cm/yr (Kreemer et al., 2014), might not be as important as the motion of the African plate prior to its slowdown *ca.* 30 Ma in imparting an anisotropic fabric to the sublithospheric mantle.

Starting in the mid-1990s, several studies, using data mainly from temporary seismic stations, expanded the number of shear wave splitting measurements, in addition to complementary observations from other seismic phases, for selected tectonic regions. Vinnik et al. (1996) reported shear wave splitting results for seven temporary stations in the Kaapvaal Craton which showed a NE ϕ direction. Silver et al. (2001), using a much larger data set from 79 temporary stations spanning the Kaapvaal and Zimbabwe cratons and the Limpopo Belt, also reported a NE ϕ direction across most of their study area. However, because the ϕ direction in most locations followed the trend of Archean structures and some changes in δt measurements correlated with tectonic terranes, Silver et al. (2001) attributed their results to anisotropy in the lithospheric mantle resulting from past tectonic events (i.e., fossil anisotropy), an interpretation consistent with xenolith studies (Ben Ismail et al., 2001) showing the lithospheric mantle beneath the Kaapvaal Craton is indeed anisotropic. Kwadiba et al. (2003), from Pn arrivals at stations used by Silver et al. (2001), reported a small but pervasive azimuthal anisotropy with a NE-SW fast direction, consistent with the Silver et al. (2001) interpretation. Vinnik et al. (2012), by jointly inverting P-wave receiver functions and SKS waveforms for the same stations used by Silver et al. (2001), argued for a multi-layer anisotropic upper mantle, with an E-W fast direction in the uppermost mantle resulting from fossil anisotropy produced by the collision between the Kaapvaal and Zimbabwe cratons, a NE ϕ direction in the asthenosphere consistent with APM, in addition a NNW to NNE ϕ direction atop the 410-km discontinuity related to a low S-velocity zone in the mantle beneath southern Africa. A similar interpretation for a NE-oriented anisotropic fabric in the asthenosphere was made by Adam and Lebedev (2012), who investigated azimuthal anisotropy using surface-wave dispersion measurements.

In more recent studies using data from temporary seismic stations in other areas of southern Africa, Yu et al. (2015) reported shear wave splitting measurements for stations traversing Botswana SE to NW and crossing the incipient Okavango Rift Zone. Their results show a strong NE ϕ orientation, which they attributed to APM. Komeazi et al. (2023) reported shear wave splitting measurements for stations in NW Namibia, attributing an observed NE ϕ direction to a combination of fossil anisotropy in the lithospheric mantle and anisotropy in the asthenosphere resulting from APM.

While these studies have significantly advanced the understanding of seismic anisotropy in southern Africa, no study to date has examined seismic anisotropy comprehensively beneath the entire region of southern Africa using shear wave splitting measurements. Here, we report new shear wave splitting measurements for 88 seismic stations in Namibia, Botswana, South Africa and Mozambique (Figure 1; Figure S1 in Supporting Information S1), greatly expanding the data set of ϕ and δt measurements for southern Africa. We combine our new measurements with 167 existing measurements (Barruol & Ben Ismail, 2001; Fouch, Silver, et al., 2004; Helffrich et al., 1994; Komeazi et al., 2023; Silver & Chan, 1991; Silver et al., 2001; Vinnik et al., 1992, 1996; Yu et al., 2015), and use the ensemble of measurements to (a) characterize the anisotropic structure of the upper mantle across southern Africa and (b) examine geodynamic processes that may have created anisotropic fabrics within the upper mantle.

2. Tectonic Background

The Precambrian shield of southern Africa is an amalgamation of cratons and mobile belts that experienced several large magmatic events during the Proterozoic and Phanerozoic, as well as periods of rifting (e.g., Begg et al., 2009; de Wit et al., 1992; Hanson, 2003; Jelsma & Dirks, 2002) (Figure 1). The oldest part of the shield, often referred to as the Kalahari Craton, consists of the Archean Kaapvaal and Zimbabwe cratons and the intervening Limpopo Belt, and is surrounded by younger terranes, *viz.* Paleoproterozoic (Kheis, Rehoboth), Mesoproterozoic (Magondi, Okwa, Namaqua-Natal, Irumide, Southern Irumide Belts), and Neoproterozoic (Damara, Gariep, Mozambique Belts) (e.g., Hofmann et al., 2013; Jacobs et al., 2008) (Figure 1). Much of southern Africa was affected by the *ca.* 180 Ma Karoo large igneous province; however, other significant magmatic events, such as the *ca.* 130 Ma Etendeka flood basalts in northwestern Namibia and the *ca.* 2.1 Ga Bushveld event in northern South Africa, may have affected more limited regions of southern Africa. Karoo rifts

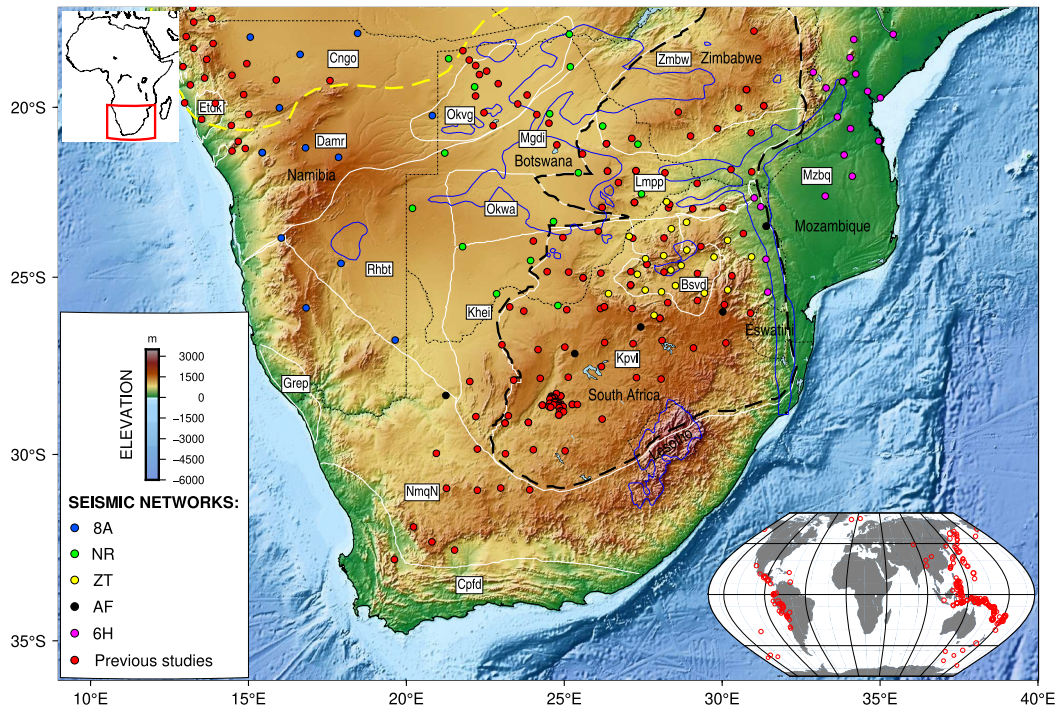

Figure 1. Topographic map showing simplified tectonic boundaries (white lines) in southern Africa, and seismic stations (colored dots) used in this study: blue, green, yellow, and magenta dots are temporary stations, black dots are permanent stations (see Figure S1 in Supporting Information S1 for station names), and red dots are stations used in previous studies. Tectonic units (white boxes): Bsvd—Bushveld Complex, Cngo—Congo Craton, Cpfd—Cape fold Belt, Damr—Damara Belt, Etdk—Etendeka Flood Basalt Province, Grep—Gariep Belt, Khei—Kheis Belt, Kpvl—Kaapvaal Craton, Lmpp—Limpopo Belt, Mgdi—Magondi Belt, Mzbq—Mozambique Belt, NmqN—Namaqua-Natal Belt, Okvg—Okavango Rift, Okwa—Okwa Terrane, Rhbt—Rehoboth Province, Zmbw—Zimbabwe Craton. Black dashed line outlines the Kalahari Craton and the yellow dashed line shows the southern margin of the Congo Craton. Blue line bounds the Karoo large igneous provinces. Thin dotted lines are political boundaries. Bottom right inset: the distribution of 223 teleseismic events (red circles) used in this study.

and sedimentary basins developed across much of southern Africa during the breakup of Gondwana, and, today, nascent rifting within the East African Rift System extends to the southwest across Zambia to the Okavango Rift Zone in northern Botswana, and to the southeast into central Mozambique (e.g., Domingues et al., 2016; Fadel et al., 2020; Fonseca et al., 2014).

3. Data and Methods

3.1. Data

Seismic data used in this study for new shear wave splitting measurements come from 17 temporary seismic stations deployed in Namibia between January 2015 and December 2018 (8A network code: https://doi.org/10.7914/SN/8A_2015), 21 temporary seismic stations deployed in Botswana between February 2013 and November 2015 (NR network code: https://doi.org/10.7914/SN/NR), 22 temporary seismic stations deployed in South Africa between January 2015 to December 2020 (ZT network code: https://doi.org/10.7914/SN/ZT_2015), and 20 temporary seismic stations deployed in Mozambique between January 2011 and December 2013 (6H network code: https://doi.org/10.7914/SN/6H_2011). In addition, data from eight permanent seismic stations located in South Africa were used (from April 1993 to present; AF network code: https://doi.org/10.7914/SN/AF). In total, data from 88 seismic stations were used in this study (Figure 1; Figure S1 and Table S1 in Supporting Information S1). Waveforms from teleseismic events with Mw $\geq$ 5.5 and epicentral distances between 90° and 140° from the seismic stations were used to measure shear wave splitting parameters (ϕ and δt). In total, data from 223 teleseismic events were used (inset Figure 1).

23335084, 2024, 5, Downloaded from https://agupubs.onlinelibrary.wiley.com/doi/10.1029/2023EA003469 by South African Medical Research, Wiley Online Library on [16/05/2024]. See the Terms and Conditions (https://onlinelibrary.wiley.com/terms-and-conditions) on Wiley Online Library for rules of use; OA articles are governed by the applicable Creative Commons License

23335084, 2024, 5, Downloaded from https://agupubs.onlinelibrary.wiley.com/doi/10.1029/2023EA003469 by South African Medical Research, Wiley Online Library on [16/05/2024]. See the Terms and Conditions (https://onlinelibrary.wiley.com/terms-and-conditions) on Wiley Online Library for rules of use; OA articles are governed by the applicable Creative Commons License

3.2. Methods

The RC and ME methods implemented in Splitlab (Wüstefeld et al., 2008) were applied to measure ϕ and δt on PKS, SKS, or SKKS phases. The seismic data were bandpass filtered between 0.02 and 0.20 Hz to minimize the influence of noise, which can lead to results with erroneously high signal-to-noise ratios (Walker et al., 2004). Figure S2 in Supporting Information S1 shows an example of an individual measurement of shear wave splitting parameters using both RC and ME methods at station NE216 in Botswana.

Sensor misorientation was suspected for several seismic stations after shear wave splitting measurements were made. For these stations, after the RC technique was applied, PKS, SKS, or SKKS energy on the transverse component was still observable, the particle motion did not show clear linearity, and the fast and slow components were poorly matched (Figure S3 in Supporting Information S1). We therefore tested for sensor misorientation by measuring the optimal orientation of the north-south component using the Rayleigh-wave polarization analysis in Stachnik et al. (2012) and compared it to the reported sensor orientation in the station metadata. An example of orientation estimation for the station OMUT is shown in Figure S4 in Supporting Information S1. Results for 24 seismic stations showed some degree of sensor misorientation (Table S2 in Supporting Information S1). The orientations of the north-south component obtained were used to correct the sensor orientations for those stations, and then ϕ and δt measurements were remade. Figure S3 in Supporting Information S1 shows an example of individual measurement of shear wave splitting parameters at station SUSS in Mozambique before and after the misorientation correction was applied to the waveforms.

We quantified and labeled all non-null measurements as "good", "fair", or "poor", using the quality factors described in Wüstefeld and Bokelmann (2007) and Andriampenomanana et al. (2021). To summarize, the measurements were checked to see if: (a) the ϕ and δt are consistent for both the RC (i.e., ϕ_{RC} and δt_{RC}) and ME (i.e., ϕ_{ME} and δt_{ME}) techniques, (b) the particle motion of the phase changed from elliptical to linear motion in the corrected signal, and (c) the energy on the transverse component was removed. Wüstefeld and Bokelmann (2007) reported an analytical approach to evaluate a shear wave splitting measurement by calculating the difference $\Delta\phi = \phi_{ME} - \phi_{RC}$ and the ratio $\rho = \delta t_{RC}/\delta t_{ME}$. In addition to criteria (b) and (c), a "good" measurement is characterized by a $|\Delta\phi| < 8°$ and $0.8 < \rho < 1.1$, a "fair" measurement if $|\Delta\phi| < 15°$ and $0.7 < \rho < 1.2$, and "poor" for the remaining measurements. Poor quality measurements were discarded.

A "null measurement", or no split, is when a PKS, SKS, or SKKS phase is observed on the radial component without any corresponding energy on the transverse component. It can be explained by the propagation of waves through an isotropic medium, or in the presence of anisotropy, the polarization is parallel to the fast or slow direction of the fast polarization direction (Savage, 1999). The latter suggests that the direction of the anisotropy is parallel or orthogonal to the event back azimuth. Following the approach of Wüstefeld and Bokelmann (2007), a "good" null measurement is characterized by a $37° < |\Delta\phi| < 53°$ and $0.0 < \rho < 0.2$, and a "near" null measurement if $32° < |\Delta\phi| < 58°$ and $0.0 < \rho < 0.3$. We only considered "good" null measurements in this study.

Individual "good" and "fair" quality non-null measurements from the ME method (Figure S5 in Supporting Information S1) were stacked using the method of Wolfe and Silver (1998) as implemented in StackSplit (Grund, 2017), to obtain a single splitting measurement (ϕ and δt) for each station. In this surface stacking approach, the error surface of each single "good" and "fair" quality non-null measurement, obtained from the ME method, is normalized either by its minimum or maximum eigenvalue of the covariance matrix of the corrected particle motion, then stacked (Grund, 2017; Wolfe & Silver, 1998). This method is well suited for obtaining shear wave splitting parameters for temporary stations, especially where the period of deployment may be insufficient to record many high-quality shear waves (Wolfe & Silver, 1998). The stacking procedure was applied only to stations with two or more individual measurements.

To assess whether more than one anisotropic layer contributes to the observed shear wave splitting parameters, modeling the observations using two anisotropic layers was attempted. Because the back azimuthal data coverage for most stations is insufficient to constrain a two-layer model, we combined measurements from stations within the same terrane, including individual measurements from previous studies (e.g., Komeazi et al., 2023; Yu et al., 2015) (Figure S6 in Supporting Information S1). Individual "good" and "fair" quality non-null measurements for stations within a terrane (Figure S6 in Supporting Information S1) were stacked in bins covering a maximum range of 5–6° with respect to back azimuth and epicentral distance using the method of Wolfe and

23335084, 2024, 5, Downloaded from https://agupubs.onlinelibrary.wiley.com/doi/10.1029/2023EA003469 by South African Medical Research, Wiley Online Library on [16/05/2024]. See the Terms and Conditions (https://onlinelibrary.wiley.com/terms-and-conditions) on Wiley Online Library for rules of use; OA articles are governed by the applicable Creative Commons License

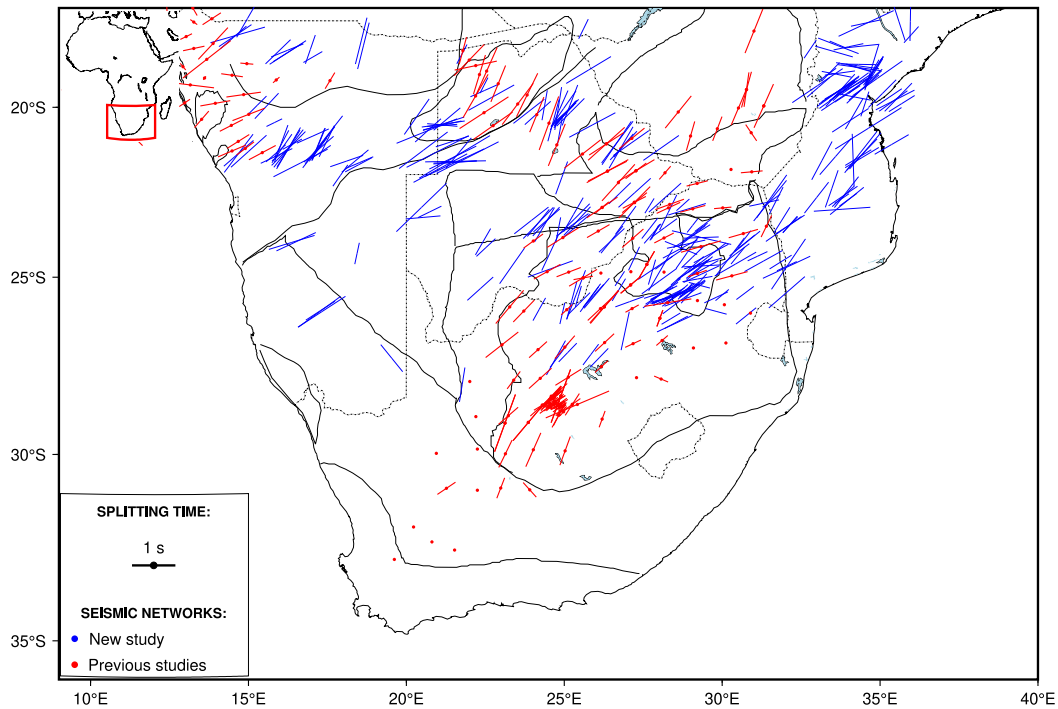

Figure 2. Individual shear wave splitting measurements (blue bars; see Table S3 in Supporting Information S1) projected at the 250 km ray piercing depth. Averaged shear wave splitting measurements in southern Africa from previous studies, plotted on the station location at the surface, are shown in red bars. The length of each line is proportional to the delay time (δt) and its direction shows the azimuth (ϕ) of the fast split shear wave measured clockwise from the north direction.

Silver (1998), as implemented in StackSplit (Grund, 2017), yielding a single splitting measurement (ϕ and δt) for each bin. Some bins only had one measurement and in those cases no stacking was performed.

The splitting parameters for each region were then modeled using the grid search approach of Grund and Ritter (2020). In this approach, the model consists of two anisotropic layers with horizontal symmetry axes (Figure S7 in Supporting Information S1). The axis in both layers was varied in 7° increments between −90° and 90°, and the delay time in 0.1 s increments between 0 and 4 s. The apparent splitting parameters were calculated for back azimuths between 0° and 360°, as described in Silver and Savage (1994), to find a model that best fits the data and minimizes the root-mean-square error between the observed and predicted splitting parameters.

4. Results and Discussion

The complete data set includes 556 individual splitting measurements (352 SKS phases, 154 SKKS phases, and 50 PKS phases), including null measurements (Table S3 in Supporting Information S1). The stacked results and the individual measurements from the 88 stations are listed in Tables S1 and S3 in Supporting Information S1, respectively. Individual measurements plotted at the projection of the ray-piercing points at a depth of 250 km are shown in Figure 2. Figure 3 shows the stacked results together with previously reported shear wave splitting measurements. Figure S8 in Supporting Information S1 shows all null measurements aligned toward the incoming back azimuth of the unsplit PKS/SKS/SKKS waves.

The amount of "good/fair" non-null and "good" null measurements per station ranges between 1 and 25 measurements, with an average of 6 measurements per station. Our new measurements, overall, show a prominent NNE to NE ϕ direction, with a ∼47° average (measured clockwise from north), and an average δt of ∼0.9 s, similar to previously reported measurements. The ensemble of measurements from previous studies (https://doi.org/10.18715/SKS_SPLITTING_DATABASE) show a ϕ that ranges between −85° and 85° with an average of 38°, and a δt that ranges between 0 and 1.7 s, with an average of 0.6 s (Figure S9 in Supporting Information S1). For all 240 stations shown in Figure 4ie, previous and new measurements), ϕ directions range between −85° and 88°, with an average of 41° (±32° SD). There are only a few exceptions where stations do not show a NNE-NE ϕ

10.1029/2023EA003469

23335084, 2024, 5, Downloaded from https://agupubs.onlinelibrary.wiley.com/doi/10.1029/2023EA003469 by South African Medical Research, Wiley Online Library on [16/05/2024]. See the Terms and Conditions (https://onlinelibrary.wiley.com/terms-and-conditions) on Wiley Online Library for rules of use; OA articles are governed by the applicable Creative Commons License

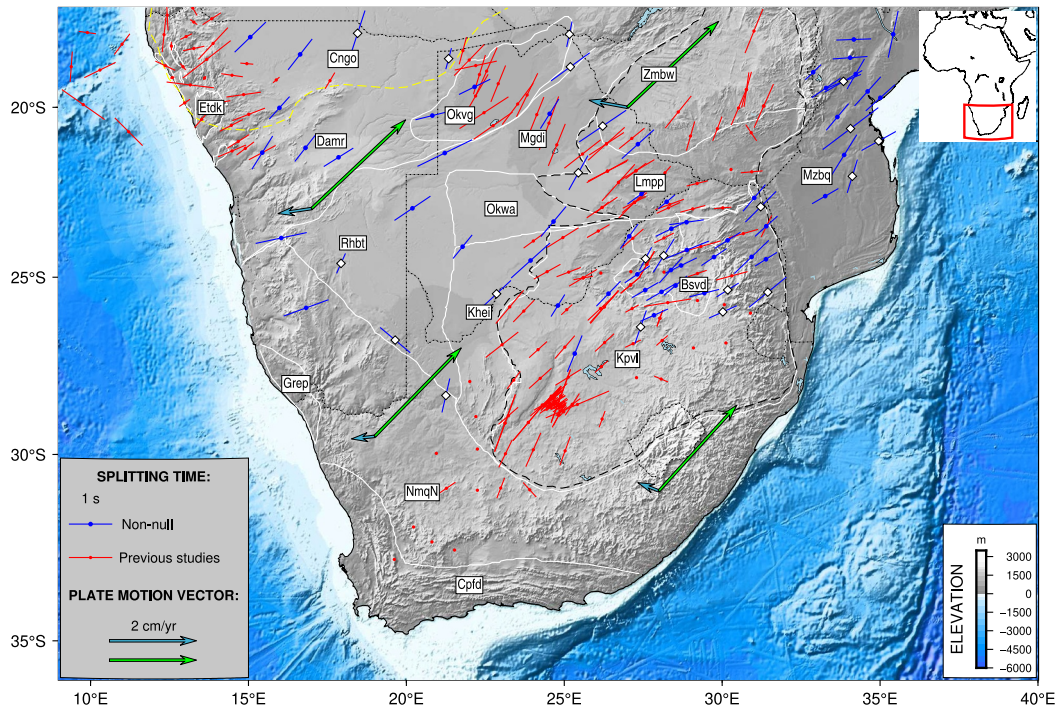

Figure 3. Shear wave splitting measurements in southern Africa from current (blue bars) and previous (red bars) studies. The length of each bar is proportional to the delay time (δt) and its direction shows the azimuth (ϕ) of the fast split shear wave measured clockwise from the north direction. White diamonds are stations that only have one single measurement. Arrows show the current plate motion vectors of the African plate the hotspot reference frame HS3-NUVEL-1A model (blue arrows) (Gripp & Gordon, 2002) and the GSRM v2.1 no-net-rotation reference frame model (green arrows) (Kreemer et al., 2014) at four random locations in southern Africa.

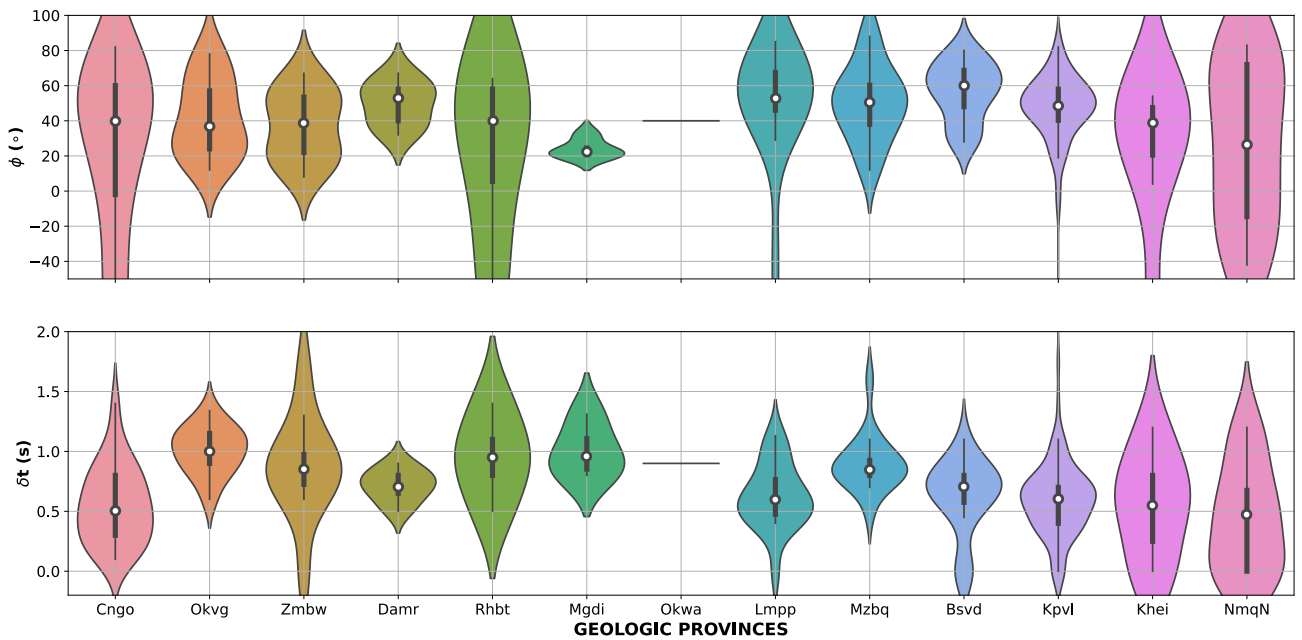

Figure 4. Violin plots showing the stacked splitting parameters (ϕ and δt) grouped by geologic terrane (provinces) for all 240 stations shown in Figure 3. The shape of each violin corresponds to the density of ϕ and δt measurements. The inner bars are box-and-whisker plots that show the data distribution *viz.* The median (white dot), lower and upper quartiles (thick black line), and minimum and maximum (thin black line). Geologic provinces (Figure 1): Cngo—Congo Craton, Okvg—Okavango Rift, Zmbw—Zimbabwe Craton, Damr—Damara Belt, Rhbt—Rehoboth Province, Mgdi—Magondi Belt, Okwa—Okwa Terrane, Lmpp—Limpopo Belt, Mzbq—Mozambique Belt, Bsvd—Bushveld Complex, Kpvl—Kaapvaal Craton, Khei—Kheis Belt, NmqN—Namaqua-Natal Belt.

23335084, 2024, 5, Downloaded from https://agupubs.onlinelibrary.wiley.com/doi/10.1029/2023EA003469 by South African Medical Research, Wiley Online Library on [16/05/2024]. See the Terms and Conditions (https://onlinelibrary.wiley.com/terms-and-conditions) on Wiley Online Library for rules of use; OA articles are governed by the applicable Creative Commons License

direction (i.e., station AROB in southeastern Namibia, station UPI in central South Africa, stations MACO and SGOR in Mozambique) (Table S1 in Supporting Information S1; Figure 3). δt values are also fairly uniform for all 240 stations, with an average of 0.7 s (±0.3 s SD) (Figure S9 in Supporting Information S1). A comparison of the mean values of the measurements between terranes in Figure 4 clearly illustrates the predominance of the NNE to NE ϕ direction across the southern African subcontinent, as well as the similarity in the distribution of ϕ and δt observations between most of the terranes. For those terranes with fewer non-null observations (i.e., Namaqua-Natal, Kheis, Rehoboth), the violin plots show a greater spread in the observations, but the terrane averages are nonetheless consistent with the averages for the other terranes.

For the null measurements at stations where non-null measurements were also obtained, we find the back azimuth of unsplit incoming PKS/SKS/SKKS waves roughly orient to the NW and NE (Figure S8 in Supporting Information S1), approximately orthogonal and parallel to the overall NNE-NE ϕ direction described above. Therefore, the null measurements at those stations can be explained by the alignment of the wave back azimuth with either the fast or slow polarization direction. There are, however, stations where only null measurements were obtained, and for these stations, the null measurements could also reflect a lesser quality and/or quantity of data compared to other stations.

Given the long and complex tectonic history of southern Africa, including many orogenic, magmatic and rifting events, it is somewhat surprising to find fairly uniform fast polarization directions and splitting times across the entire region (Figures 2 and 3; Figure S8 in Supporting Information S1). Is it possible that there is just one source of mantle anisotropy that gives rise to the fairly uniform ϕ and δt pattern observed, or alternatively, is it possible that two or more sources created the observed pattern? Following from the previous studies that have invoked either flow in the sublithospheric mantle and/or fossil anisotropy within the mantle lithosphere (see Section 1 for review), we first examine mantle flow associated with plate motion to address that question, then investigate fossil anisotropy within the mantle lithosphere, and finally evaluate if anisotropy in both the lithospheric and sub-lithospheric mantle can together explain the NNE-NE fast polarization direction. We note that because there is no Cenozoic volcanism within the study area, invoking SPO from aligned inclusions or pockets of melt to explain the shear wave splitting observations is not tectonically realistic.

4.1. Shear in the Asthenosphere From Plate Motion

The movement of the rigid lithosphere over the asthenosphere reorients the fast axis (a-axis) of olivine, imparting an LPO-induced anisotropy in the asthenosphere with ϕ parallel to the direction of the overriding plate (i.e., APM parallel anisotropy) (Savage, 1999). This source of anisotropy is typically invoked when the ϕ pattern shows similarity to the APM direction. The compilation of shear wave splitting measurements showing an average ϕ of 41° (Figure 3), which is similar to the plate motion direction in GSRM v2.1 no-net-rotation reference frame model (Kreemer et al., 2014), suggests that APM could cause the NNE-NE ϕ pattern, as originally proposed by Vinnik et al. (1995). However, as noted by Barruol and Ben Ismail (2001), given how slowly the African plate has been moving for the past 30 Ma (Argus et al., 2011; Gripp & Gordon, 2002; Kreemer et al., 2014), the NNE-NE ϕ pattern may also reflect APM prior to 30 Ma when the plate moved relatively faster. Several hotspot tracks on the African plate, showing a NE orientation (Figure 5), record its direction and speed prior to the slowdown (e.g., Duncan, 1981; Duncan & Richards, 1991; Summerfield, 1996). This leads to the possibility that an LPO fabric oriented to the NE may also have developed in the sublithospheric mantle beneath southern Africa, as well as the rest of the African plate, when the plate was moving at a faster velocity prior to *ca.* 30 Ma.

4.2. Upper Mantle Flow From the African Superplume

Next, we examine if flow in the upper mantle induced by the African Superplume can provide a viable explanation for the NNE-NE ϕ direction through LPO-induced anisotropy. The African Superplume is a large lower mantle thermo-chemical structure under southern Africa that appears to rise into the mid-mantle to the NE beneath Zambia and continues into the upper mantle beneath eastern Africa (e.g., Adams et al., 2012; Hansen et al., 2012; Mulibo & Nyblade, 2013; O'Donnell et al., 2013; Simmons et al., 2007, 2011; Tsekhmistrenko et al., 2021), and may be a long-lived feature of the Phanerozoic African mantle (Torsvik et al., 2010). Upper mantle flow to the NE beneath eastern Africa associated with the African Superplume has been used to explain a similar NE ϕ direction observed throughout much of eastern Africa (Andriampenomanana et al., 2021; Bagley & Nyblade, 2013; Forte et al., 2010).

10.1029/2023EA003469

23335084, 2024, 5, Downloaded from https://agupubs.onlinelibrary.wiley.com/doi/10.1029/2023EA003469 by South African Medical Research, Wiley Online Library on [16/05/2024]. See the Terms and Conditions (https://onlinelibrary.wiley.com/terms-and-conditions) on Wiley Online Library for rules of use; OA articles are governed by the applicable Creative Commons License

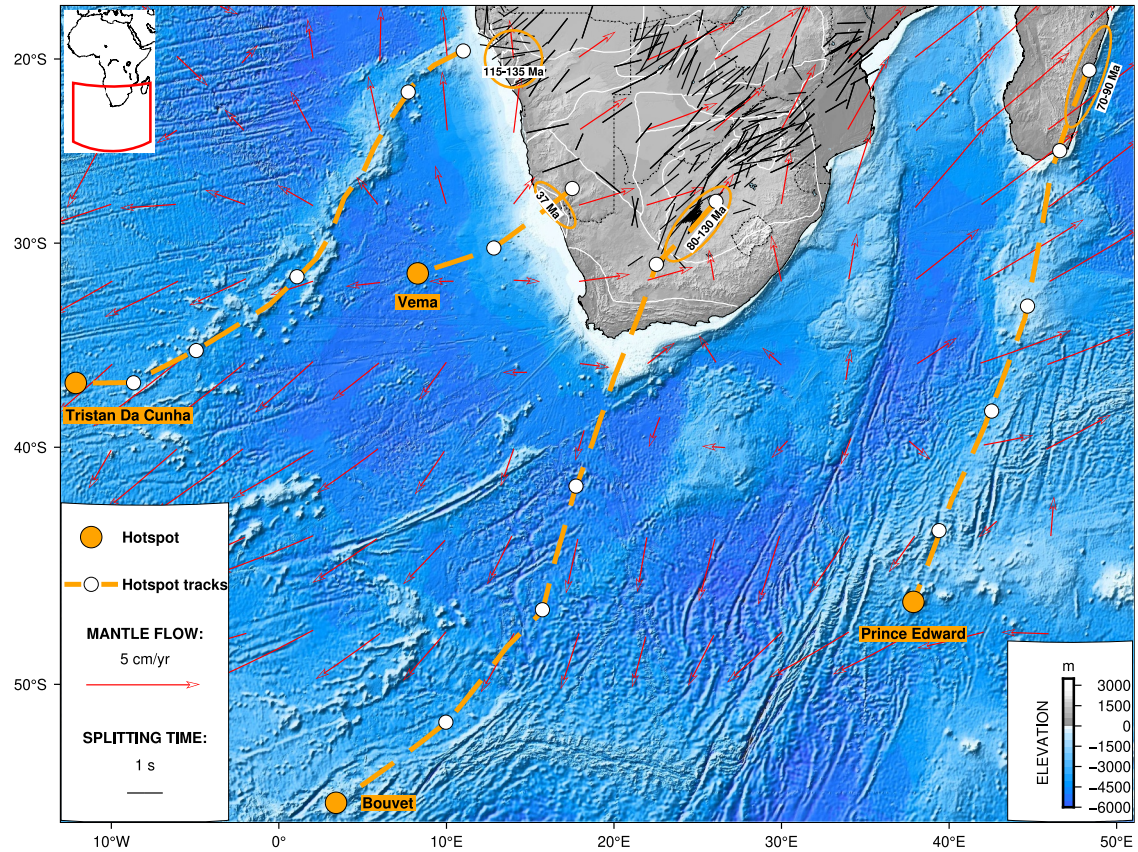

Figure 5. Map showing the shear wave splitting measurements in southern Africa from this and previous studies along with the predicted horizontal flow at depth of 250 km in the upper mantle from Forte et al. (2010) (red arrows). Hotspots and tracks from Duncan (1981) are shown with orange dashed lines. Orange ovals with ages show the location and timing of the initial hotspot volcanism, and the white circles are at 20 Ma age increments along each track. White lines show same terrane boundaries as in Figure 1.

Figure 5 shows horizontal flow directions in the upper mantle beneath southern Africa at 250 km depth induced by the superplume structure derived from the instantaneous mantle flow model of Forte et al. (2010). The predicted horizontal flow shows an overall NE flow direction, but the pattern is not uniform across southern Africa, and in some areas, for example, northern Namibia and southern South Africa, the flow directions are more northerly or easterly. The predicted flow pattern only provides a good match with the ϕ direction in some regions. Therefore, when flow induced by the superplume is considered by itself, it may not provide a robust explanation for the observed NNE-NE ϕ pattern, but in combination with other sources of anisotropy, it could contribute to the pattern.

4.3. Fossil Anisotropy

The other explanation for the NNE-NE ϕ pattern mentioned above is fossil anisotropy in the lithospheric mantle. The lithosphere across southern Africa is everywhere 100–125 km thick or thicker (e.g., Fishwick, 2010; Fouch, James, et al., 2004; Miensopust et al., 2011; White-Gaynor et al., 2020), sufficiently thick to give rise to a δt of 0.7 s or more (e.g., Silver & Chan, 1991). As reviewed in Section 2, there have been many orogenic events through the Precambrian that could have led to an LPO anisotropic fabric in the lithospheric mantle, and for each event, it would be expected that the ϕ direction would be oriented perpendicular to the collision direction. The orientation of terrane boundaries and collision directions vary considerably across southern Africa (e.g., Begg et al., 2009), and thus it seems highly unlikely that a NNE-NE ϕ direction would have resulted from multiple orogenic events over a period of more than 2 Ga. Therefore, we do not favor invoking only fossil anisotropy in the mantle lithosphere from multiple past collisional events to explain the NNE-NE ϕ direction.

However, the last major orogenic event within the interior of southern Africa was the *ca.* 580–543 Ma formation of the Damara Belt resulting from the collision of the Kalahari and Congo cratons. The NE orientation of the

23335084, 2024, 5, Downloaded from https://agupubs.onlinelibrary.wiley.com/doi/10.1029/2023EA003469 by South African Medical Research, Wiley Online Library on [16/05/2024]. See the Terms and Conditions (https://onlinelibrary.wiley.com/terms-and-conditions) on Wiley Online Library for rules of use; OA articles are governed by the applicable Creative Commons License

Damara Belt (Figure 1), which is orthogonal to the collision direction between the cratons, aligns well with the NNE-NE ϕ direction. We thus propose that this final major orogenic event in the formation of the southern African Precambrian Shield may have imparted a NE oriented anisotropic fabric to the lithospheric mantle across much of the region, overprinting fabrics imparted to the lithospheric mantle by earlier orogenic events.

Figure 4 illustrates a range of fast polarization directions within each terrane around the average NNE-NE direction. Some of the variability between terranes could reflect only partial resetting of previously developed fossil anisotropic fabrics within the lithospheric mantle. For example, in the Limpopo Belt, there are localized anisotropic patterns consistent with the surface geologic features from an older orogenic event. A clockwise rotation of fast polarization directions, subparallel to the trend of the arc that spans the Limpopo Belt, the northeastern region of the Kaapvaal Craton, and the Bushveld Complex, has been previously observed and explained with fossil anisotropy that resides within the lithospheric mantle arising from the collision of the Kaapvaal and Zimbabwe cratons *ca.* 2.9–2.6 Ga (Silver et al., 2004). The newly reported shear wave splitting measurements also show a ϕ pattern subparallel to the collisional arc across the area, similar to the pattern reported by Silver et al. (2004). Therefore, anisotropy in the lithosphere beneath the Limpopo Belt may have been only partially modified during the Damara orogeny.

4.4. Two or More Anisotropic Layers

Given that anisotropic fabrics could have developed in both the lithospheric and sublithospheric mantle, as discussed above, there is a possibility that anisotropy in two or more layers could be combining to create to the NNE-NE ϕ pattern. The anisotropy pattern resulting from two anisotropic layers with horizontal symmetry axes typically displays a $\pi/2$ periodicity (Silver & Savage, 1994), and with sufficient back azimuthal data coverage, such a pattern can be constrained and used to model ϕ and δt in each layer.

As mentioned in Section 3.2, the data available for each station used in this study have limited back azimuthal coverage and do not constrain a $\pi/2$ periodicity (Figure S5 in Supporting Information S1). Therefore, modeling multiple layers of anisotropy for individual stations has not been undertaken. However, by combining observations from stations within a terrane, it might be possible to constrain a two-layer model reflective of anisotropic conditions across a terrane (Figure S6 in Supporting Information S1), with the top layer representing fossil anisotropy in the lithosphere and the bottom layer LPO-induced anisotropy in the asthenosphere (Figure S7 in Supporting Information S1).

The results of this approach for terranes with the best back azimuthal data coverage are shown in Figure S10 in Supporting Information S1. For these terranes, the back azimuthal data coverage, however, remains limited and does not clearly show a $\pi/2$ periodicity. This reflects the locations of the main earthquake source regions for southern Africa in the appropriate distance range, which lie between about 45 and 140° back azimuth (Pacific subduction zones) and about 240–300° back azimuth (southern South American subduction zone). The shear wave splitting observations can be fit equally well with a one-layer model, and therefore it is difficult to use results from two-layer modeling to draw firm conclusions about the relative contributions from the lithospheric and sublithospheric mantle to the overall NNE-NE ϕ pattern. Nonetheless, it is interesting to note that in the two-layer models, the lower and upper layers exhibit a similar range of ϕ directions (1°–78° for lower layer; 15°–78° for upper layer; Figure S10 in Supporting Information S1). We also note that allowing the fast axis of the anisotropy in one or both layers to have a non-zero plunge, which would no longer necessarily produce observational patterns with a $\pi/2$ periodicity, could possibly produce models that fit the data better.

An additional complication in attributing the NNE-NE ϕ direction to more than one anisotropic layer is presented by studies suggesting the lowermost mantle beneath parts of Africa may also be anisotropic. For example, an anisotropic layer at the margins of the African large low shear velocity province associated with mantle flow in the D" region has been identified (Lynner & Long, 2014; Pisconti et al., 2023; Reiss et al., 2019). If a third source of anisotropy in the mantle beneath southern Africa exists, then unraveling the layer contributions to the observed NNE-NE ϕ pattern becomes even more challenging given the limited back azimuthal data coverage.

5. Summary and Conclusion

To summarize, the ensemble of shear wave splitting measurements from 240 seismic stations spread across southern Africa reveal a fairly uniform pattern, with a predominant NNE-NE ϕ direction, with an average ϕ of 41°

23335084, 2024, 5, Downloaded from https://agupubs.onlinelibrary.wiley.com/doi/10.1029/2023EA003469 by South African Medical Research, Wiley Online Library on [16/05/2024]. See the Terms and Conditions (https://onlinelibrary.wiley.com/terms-and-conditions) on Wiley Online Library for rules of use; OA articles are governed by the applicable Creative Commons License

and average δt of 0.7 s. The NNE-NE ϕ direction was evident in previous shear wave splitting studies in selected parts of southern Africa. The results of this study show the NNE-NE ϕ direction is characteristic of the entire southern African subcontinent.

Given the complex >3 Ga tectonic history of the southern Africa, with many orogenic belts and cratons, it is unlikely the predominant NNE-NE ϕ direction could arise only from fossil anisotropy imparted to the mantle lithosphere by orogenic events. And it is also unlikely that flow in the sublithospheric mantle induced by the African Superplume could, by itself, lead to the predominant NNE-NE ϕ direction. However, it is possible that the NNE-NE ϕ direction could result from APM, or else from the last major orogenic event within the interior of southern Africa, the *ca.* 580–543 Ma formation of the Damara Belt, which could have created a widespread NE-oriented anisotropic fabric in much of the lithospheric mantle in southern Africa.

Alternatively, we propose the prominent NNE-NE ϕ direction in southern Africa is the combined expression of several processes which have created similarly oriented anisotropic fabrics in the lithospheric and sublithospheric upper mantle; that is, APM (present and past), fossil anisotropy from the Neoproterozoic collision of the Congo and Kalahari cratons and possibly other Precambrian orogenic events, and mantle flow induced by the African Superplume. Indeed, the robustness of the observed NNE-NE ϕ pattern across such a large region of the African continent lends support to the possibility of contributions to the splitting of shear waves from two or more regions of the upper mantle with similar anisotropic fabrics. It is also possible that localized departures from the NNE-NE ϕ direction in some places may reflect the influence of additional anisotropic fabrics in the lithospheric mantle that were not completely overprinted by the Neoproterozoic tectonism during the formation of the Damara Belt, and/or the influence of small-scale flow in the sublithospheric mantle arising from variations in lithospheric thickness or complexities in superplume-induced mantle flow. In addition, a contribution from anisotropy in the lowermost mantle in the vicinity of the African large low shear velocity province cannot be ruled out.

Data Availability Statement

Data used in this study were downloaded from the IRIS Data Management Center (IRISDMC). Network code 8A (Nyblade, 2015a, 2015b): https://doi.org/10.7914/SN/8A_2015; network code NR (Utrecht University, 1983 (UU Netherlands)): https://doi.org/10.7914/SN/NR; network code ZT (Nyblade, 2015a, 2015b): https://doi.org/10.7914/SN/ZT_2015, network code 6H (Helffrich & Fonseca, 2011): https://doi.org/10.7914/SN/6H_2011; and network code AF (Penn State University, 2004): https://doi.org/10.7914/SN/AF. Splitlab (Wüstefeld et al., 2008) was utilized to measure the splitting parameters, and StackSplit (Grund, 2017) was used to stack individual measurements. Two-layer modeling was conducted using the shear wave splitting modeling package developed by Grund and Ritter (2020). Citations for these tools are provided in the references section.

Acknowledgments

This work was supported by Grant ALW-GO-AO/11-30 provided by Nederlandse Organisatie voor Wetenschappelijk Onderzoek (NWO) and National Science Foundation Grants 0440032, 0530062, 0824781, 1128936, and 1634108. The support of the National Research Foundation through the South African Research Chairs Initiative is also acknowledged. We also acknowledge the efforts of staff at the Botswana Geological Survey, the Namibia Geological Survey, and the Council for Geoscience (South Africa) for installing and maintaining seismic stations, and the IRIS Passcal Instrument Center for providing seismic equipment and field support. We thank Judith Confal and Karen Fischer for providing insightful reviews which helped to improve the paper. Figures in this paper have been produced with GMT (Wessel & Smith, 1998).

References

Adam, J. M.-C., & Lebedev, S. (2012). Azimuthal anisotropy beneath southern Africa from very broad-band surface-wave dispersion measurements. *Geophysical Journal International*, *191*(1), 155–174. https://doi.org/10.1111/j.1365-246x.2012.05583.x

Adams, A., Nyblade, A. A., & Weeraratne, D. (2012). Upper mantle shear wave velocity structure beneath the East African plateau: Evidence for a deep, plateau wide low velocity anomaly. *Geophysical Journal International*, *189*(1), 123–142. https://doi.org/10.1111/j.1365-246x.2012.05373.x

Andriampenomanana, F., Nyblade, A. A., Durrheim, R. J., Tugume, F., & Nyago, J. (2021). Shear wave splitting measurements in northeastern Uganda and southeastern Tanzania: Corroborating evidence for sublithospheric mantle flow beneath East Africa. *Geophysical Journal International*, *226*(3), 1696–1704. https://doi.org/10.1093/gji/ggab167

Argus, D. F., Gordon, R. G., & DeMets, C. (2011). Geologically current motion of 56 plates relative to the no-net-rotation reference frame. *Geochemistry, Geophysics, Geosystems*, *12*(11), Q11001. https://doi.org/10.1029/2011gc003751

Bagley, B., & Nyblade, A. A. (2013). Seismic anisotropy in eastern Africa, mantle flow, and the African superplume. *Geophysical Research Letters*, *40*(8), 1500–1505. https://doi.org/10.1002/grl.50315

Barruol, G., & Ben Ismail, W. (2001). Upper mantle anisotropy beneath the African IRIS and Geoscope stations. *Geophysical Journal International*, *146*(2), 549–561. https://doi.org/10.1046/j.0956-540x.2001.01481.x

Begg, G. C., Griffin, W. L., Natapov, L. M., O'Reilly, S. Y., Grand, S. P., O'Neill, C. J., et al. (2009). The lithospheric architecture of Africa: Seismic tomography, mantle petrology, and tectonic evolution. *Geosphere*, *5*(1), 23–50. https://doi.org/10.1130/ges00179.s1

Ben Ismail, W., Barruol, G., & Mainprice, D. (2001). The Kaapvaal craton seismic anisotropy: Petrophysical analyses of upper mantle kimberlite nodules. *Geophysical Research Letters*, *28*(13), 2497–2500. https://doi.org/10.1029/2000gl012419

Bowman, J. R., & Ando, M. (1987). Shear-wave splitting in the upper-mantle wedge above the Tonga subduction zone. *Geophysical Journal of the Royal Astronomical Society*, *88*(1), 25–41. https://doi.org/10.1111/j.1365-246x.1987.tb01367.x

de Wit, M. J., Jones, M. G., & Buchanan, D. L. (1992). The geology and tectonic evolution of the Pietersburg greenstone belt, South Africa. *Precambrian Research*, *55*(1–4), 123–153. https://doi.org/10.1016/0301-9268(92)90019-k

Domingues, A., Silveira, G., Ferreira, A. M. G., Chang, S., Custódio, S., & Fonseca, J. F. B. D. (2016). Ambient noise tomography of the East African rift in Mozambique. *Geophysical Journal International*, *204*(3), 1565–1578. https://doi.org/10.1093/gji/ggv538

Duncan, R. A. (1981). Hotspots in the southern oceans – An absolute frame of reference for motion of the Gondwana continents. In S. C. Solomon, R. Var der Voo, & M. A. Chinnery (Eds.), *Quantitative methods of assessing plate motions* (Vol. 74, pp. 29–42). Tectonophysics.

Duncan, R. A., & Richards, M. A. (1991). Hotspots, mantle plumes, flood basalts, and true polar wander. *Reviews of Geophysics*, *29*(1), 31–50. https://doi.org/10.1029/90rg02372

Fadel, I., Paulssen, H., van der Meijde, M., Kwadiba, M., Ntibinyane, O., Nyblade, A. A., & Durrheim, R. (2020). Crustal and upper mantle shear wave velocity structure of Botswana: The 3 April 2017 central Botswana earthquake linked to the East African Rift System. *Geophysical Research Letters*, *47*(4), e2019GL085598. https://doi.org/10.1029/2019gl085598

Fishwick, S. (2010). Surface wave tomography: Imaging of the lithosphere asthenosphere boundary beneath central and southern Africa. *Lithos*, *120*(1–2), 63–73. https://doi.org/10.1016/j.lithos.2010.05.011

Fonseca, J. F. B. D., Chamussa, J., Domingues, A., Helffrich, G., Antunes, E., van Aswegen, G., et al. (2014). MOZART: A seismological investigation of the East African Rift in central Mozambique. *Seismological Research Letters*, *85*(1), 108–116. https://doi.org/10.1785/0220130082

Forte, A. M., Quéré, S., Moucha, R., Simmons, N. A., Grand, S. P., Mitrovica, J. X., & Rowley, D. B. (2010). Joint seismic-geodynamic-mineral physical modeling of African geodynamics: A reconciliation of deep mantle convection with surface geophysical constraints. *Earth and Planetary Science Letters*, *295*(3–4), 329–341. https://doi.org/10.1016/j.epsl.2010.03.017

Fouch, M. J., James, D. E., VanDecar, J. C., & van der Lee, S., & Kaapvaal Seismic Group. (2004). Mantle seismic structure beneath the Kaapvaal and Zimbabwe cratons. *South African Journal of Geology*, *107*(1–2), 33–44. https://doi.org/10.2113/107.1-2.33

Fouch, M. J., Silver, P. G., Bell, D. R., & Lee, J. N. (2004). Small-scale variations in seismic anisotropy near Kimberley, South Africa. *Geophysical Journal International*, *157*(2), 764–774. https://doi.org/10.1111/j.1365-246x.2004.02234.x

Gripp, A. E., & Gordon, R. G. (2002). Young tracks of hotspots and current plate velocities. *Geophysical Journal International*, *150*(2), 321–361. https://doi.org/10.1046/j.1365-246x.2002.01627.x

Grund, M. (2017). StackSplit—A plugin for multi-event shear wave splitting analyses in SplitLab [Software]. *Computers and Geosciences*, *105*, 43–50. https://doi.org/10.1016/j.cageo.2017.04.015

Grund, M., & Ritter, J. R. R. (2020). Shear-wave splitting beneath Fennoscandia – Evidence for dipping structures and laterally varying multilayer anisotropy [Software]. *Geophysical Journal International*, *223*(3), 1525–1547. https://doi.org/10.1093/gji/ggaa388

Hansen, S. E., Nyblade, A. A., & Benoit, M. H. (2012). Mantle structure beneath Africa and Arabia from adaptively parameterized P-wave tomography: Implications for the origin of Cenozoic Afro-Arabian tectonism. *Earth and Planetary Science Letters*, *319–320*, 23–34. https://doi.org/10.1016/j.epsl.2011.12.023

Hanson, R. E. (2003). Proterozoic geochronology and tectonic evolution of southern Africa. *Geological Society, London, Special Publications*, *206*(1), 427–463. https://doi.org/10.1144/gsl.sp.2003.206.01.20

Helffrich, G., & Fonseca, J. F. B. D. (2011). Mozambique rift tomography [Dataset]. *International Federation of Digital Seismograph Networks*. https://doi.org/10.7914/SN/6H_2011

Helffrich, G., Silver, P., & Given, H. (1994). Shear-wave splitting variation over short spatial scales on continents. *Geophysical Journal International*, *119*(2), 561–573. https://doi.org/10.1111/j.1365-246x.1994.tb00142.x

Hofmann, M., Linnemann, U., Hoffmann, K.-H., Gerdes, A., Eckelmann, K., & Gärtner, A. (2013). The namuskluft and dreigratberg sections in southern Namibia (Kalahari craton, Gariep belt): A geological history of Neoproterozoic rifting and recycling of cratonic crust during the dispersal of Rodinia until the amalgamation of Gondwana. *International Journal of Earth Sciences*, *103*(5), 1187–1202. https://doi.org/10.1007/s00531-013-0949-6

Jacobs, J., Pisarevsky, S., Thomas, R. J., & Becker, T. (2008). The Kalahari craton during the assembly and dispersal of Rodinia. *Precambrian Research*, *160*(1–2), 142–158. https://doi.org/10.1016/j.precamres.2007.04.022

Jelsma, H. A., & Dirks, P. H. (2002). Neoarchaean tectonic evolution of the Zimbabwe Craton. *Geological Society, London, Special Publications*, *199*(1), 183–211. https://doi.org/10.1144/gsl.sp.2002.199.01.10

Kendall, J.-M., Pilidou, S., Keir, D., Bastow, I. D., Stuart, G. W., & Ayele, A. (2006). Mantle upwellings, melt migration and the rifting of Africa: Insights from seismic anisotropy. *Geological Society, London, Special Publications*, *259*(1), 55–72. https://doi.org/10.1144/gsl.sp.2006.259.01.06

Komeazi, A., Kaviani, A., & Rümpker, G. (2023). Mantle anisotropy in NW Namibia from XKS splitting: Effects of asthenospheric flow, lithospheric structures, and magmatic underplating. *Geophysical Research Letters*, *50*(3), e2022GL102119. https://doi.org/10.1029/2022gl102119

Kreemer, C., Blewitt, G., & Klein, E. C. (2014). A geodetic plate motion and global strain rate model. *Geochemistry, Geophysics, Geosystems*, *15*(10), 3849–3889. https://doi.org/10.1002/2014gc005407

Kwadiba, M. T. O. G., Wright, C., Kgaswane, E. M., Simon, R. E., & Nguuri, T. K. (2003). Pn arrivals and lateral variations of Moho geometry beneath the Kaapvaal craton. *Lithos*, *71*(2–4), 393–411. https://doi.org/10.1016/j.lithos.2003.07.008

Lynner, C., & Long, M. D. (2014). Lowermost mantle anisotropy and deformation along the boundary of the African LLSVP. *Geophysical Research Letters*, *41*(10), 3447–3454. https://doi.org/10.1002/2014gl059875

Miensopust, M. P., Jones, A. G., Muller, M. R., Garcia, X., & Evans, R. L. (2011). Lithospheric structures and Precambrian terrane boundaries in northeastern Botswana revealed through magnetotelluric profiling as part of the southern African magnetotelluric experiment. *Journal of Geophysical Research*, *116*(B2), B02401. https://doi.org/10.1029/2010jb007740

Mulibo, D. M., & Nyblade, A. A. (2013). The P and S wave velocity structure of the mantle beneath eastern Africa and the African superplume anomaly. *Geochemistry, Geophysics, Geosystems*, *14*(8), 2696–2715. https://doi.org/10.1002/ggge.20150

Nicolas, A., & Christensen, N. I. (1987). Formation of anisotropy in upper mantle peridotites - a review. *Reviews of Geophysics*, *25*(1987), 111–123. https://doi.org/10.1029/gd016p0111

Nyblade, A. A. (2015a). AfricaArray–Namibia [Dataset]. *IRIS*. https://doi.org/10.7914/SN/8A_2015

Nyblade, A. A. (2015b). REU: Imaging the Bushveld complex, South Africa [Dataset]. *International Federation of Digital Seismograph Networks*. https://doi.org/10.7914/SN/ZT_2015

O'Donnell, J. P., Adams, A., Nyblade, A. A., Mulibo, G. D., & Tugume, F. (2013). The uppermost mantle shear wave velocity structure of eastern Africa from Rayleigh wave tomography: Constraints on rift evolution. *Geophysical Journal International*, *194*(2), 961–978. https://doi.org/10.1093/gji/ggt135

Penn State University. (2004). AfricaArray [Dataset]. *International Federation of Digital Seismograph Networks*. https://doi.org/10.7914/SN/AF

Pisconti, A., Creasy, N., Wookey, J., Long, M. D., & Thomas, C. (2023). Mineralogy, fabric, and deformation domains in D" across the southwestern border of the African LLSVP. *Geophysical Journal International*, *232*(1), 705–724. https://doi.org/10.1093/gji/ggac359

Reiss, M. C., Long, M. D., & Creasy, N. (2019). Lowermost mantle anisotropy beneath Africa from differential SKS-SKKS shear-wave splitting. *Journal of Geophysical Research*, *124*(8), 8540–8564. https://doi.org/10.1029/2018jb017160

23335084, 2024, 5, Downloaded from https://agupubs.onlinelibrary.wiley.com/doi/10.1029/2023EA003469 by South African Medical Research, Wiley Online Library on [16/05/2024]. See the Terms and Conditions (https://onlinelibrary.wiley.com/terms-and-conditions) on Wiley Online Library for rules of use; OA articles are governed by the applicable Creative Commons License

Savage, M. K. (1999). Seismic anisotropy and mantle deformation: What have we learned from shear wave splitting? *Reviews of Geophysics*, *37*(1), 65–106. https://doi.org/10.1029/98rg02075

Silver, P. G., & Chan, W. W. (1991). Shear wave splitting and subcontinental mantle deformation. *Journal of Geophysical Research*, *96*(B10), 16429–16454. https://doi.org/10.1029/91jb00899

Silver, P. G., Fouch, M. J., Gao, S. S., & Schmitz, M., & the Kaapvaal Seismic Group. (2004). Seismic anisotropy, mantle fabric, and the magmatic evolution of Precambrian southern Africa. *South African Journal of Geology*, *107*(1–2), 45–58. https://doi.org/10.2113/107.1-2.45

Silver, P. G., Gao, S. S., Liu, K. H., & The Kaapvaal Seismic Group. (2001). Mantle deformation beneath southern Africa. *Geophysical Research Letters*, *28*(13), 2493–2496. https://doi.org/10.1029/2000gl012696

Silver, P. G., & Savage, M. K. (1994). The interpretation of shear-wave splitting parameters in the presence of two anisotropic layers. *Geophysical Journal International*, *119*(3), 949–963. https://doi.org/10.1111/j.1365-246x.1994.tb04027.x

Simmons, N. A., Forte, A. M., & Grand, S. P. (2007). Thermochemical structure and dynamics of the African superplume. *Geophysical Research Letters*, *34*(2), L02301. https://doi.org/10.1029/2006gl028009

Simmons, N. A., Myers, S. C., & Johannesson, G. (2011). Global-scale P wave tomography optimized for prediction of teleseismic and regional travel times for Middle East events: 2. Tomographic inversion. *Journal of Geophysical Research*, *116*(B4), B04305. https://doi.org/10.1029/2010jb007969

Stachnik, J. C., Sheehan, A. F., Zietlow, D. W., Yang, Z., Collins, J., & Ferris, A. (2012). Determination of New Zealand ocean bottom seismometer orientation via Rayleigh-wave polarization. *Seismological Research Letters*, *83*(4), 704–713. https://doi.org/10.1785/0220110128

Summerfield, M. A. (1996). Tectonics, geology and long-term landscape development. In W. M. Adams, A. S. Goudie, & A. R. Orme (Eds.), *The physical geography of Africa* (pp. 1–17). Oxford Univ. Press.

Torsvik, T. H., Burke, K., Steinberger, B., Webb, S. J., & Ashwal, L. D. (2010). Diamonds sampled by plumes from the core-mantle boundary. *Nature*, *466*(7304), 352–355. https://doi.org/10.1038/nature09216

Tsekhmistrenko, M., Sigloch, K., Hosseini, K., & Barruol, G. (2021). A tree of Indo-African mantle plumes imaged by seismic tomography. *Nature Geoscience*, *14*(8), 612–619. https://doi.org/10.1038/s41561-021-00762-9

Utrecht University (UU Netherlands). (1983). NARS [Dataset]. *International Federation of Digital Seismograph Networks*. https://doi.org/10.7914/SN/NR

Vinnik, L., Kiselev, M., Weber, M., Oreshin, S., & Makeyeva, L. (2012). Frozen and active seismic anisotropy beneath sourthern Africa. *Geophysical Research Letters*, *39*(8), L08301. https://doi.org/10.1029/2012gl051326

Vinnik, L. P., Green, R. W. E., & Nicolaysen, L. O. (1995). Recent deformation of the deep continental root beneath southern Africa. *Nature*, *375*(6526), 50–52. https://doi.org/10.1038/375050a0

Vinnik, L. P., Green, R. W. E., & Nicolaysen, L. O. (1996). Seismic constraints on dynamics of the mantle of the Kaapvaal. *Physics of the Earth and Planetary Interiors*, *95*(3–4), 139–151. https://doi.org/10.1016/0031-9201(95)03123-5

Vinnik, L. P., Makeyeva, L. I., Milev, A., & Yu. Usenko, A. (1992). Global patterns of azimuthal anisotropy and deformations in the continental mantle. *Geophysical Journal International*, *111*(3), 433–447. https://doi.org/10.1111/j.1365-246x.1992.tb02102.x

Walker, K. T., Nyblade, A. A., Klemperer, S. L., Bokelmann, G. H. R., & Owens, T. J. (2004). On the relationship between extension and anisotropy: Constraints from shear wave splitting across the East African plateau. *Journal of Geophysical Research*, *109*(B18), 8302. https://doi.org/10.1029/2003jb002866

Wessel, P., & Smith, W. H. (1998). New, improved version of generic mapping tools released. *EOS, Transactions American Geophysical Union*, *79*(47), 579.

White-Gaynor, A. L., Nyblade, A. A., Durrheim, R. J., Raveloson, R., van der Meijde, M., Fadel, I., et al. (2020). Lithospheric boundaries and upper mantle structure beneath southern Africa imaged by P and S wave velocity models. *Geochemistry, Geophysics, Geosystems*, *21*(10), e2020GC008925. https://doi.org/10.1029/2020gc008925

Wolfe, C. J., & Silver, P. G. (1998). Seismic anisotropy of oceanic upper mantle: Shear wave splitting methodologies and observations. *Journal of Geophysical Research*, *103*(B1), 749–772. https://doi.org/10.1029/97jb02023

Wüstefeld, A., & Bokelmann, G. (2007). Null detection in shear-wave splitting measurements. *Bulletin of the Seismological Society of America*, *97*(4), 1204–1211. https://doi.org/10.1785/0120060190

Wüstefeld, A., Bokelmann, G., Zaroli, C., & Barruol, G. (2008). SplitLab: A shear-wave splitting environment in Matlab [Software]. *Computers and Geosciences*, *34*(5), 515–528. https://doi.org/10.1016/j.cageo.2007.08.002

Yu, Y., Gao, S. S., Moidaki, M., Reed, C. A., & Liu, K. H. (2015). Seismic anisotropy beneath the incipient Okavango rift: Implications for rifting initiation. *Earth and Planetary Science Letters*, *430*, 1–8. https://doi.org/10.1016/j.epsl.2015.08.009

23335084, 2024, 5, Downloaded from https://agupubs.onlinelibrary.wiley.com/doi/10.1029/2023EA003469 by South African Medical Research, Wiley Online Library on [16/05/2024]. See the Terms and Conditions (https://onlinelibrary.wiley.com/terms-and-conditions) on Wiley Online Library for rules of use; OA articles are governed by the applicable Creative Commons License